












Mycobacterial surface characters remodeled by growth conditions drive different tumor-infiltrating cells and systemic IFN- γ /IL-17 release in bladder cancer treatment

Sandra Guallar-Garrido ^a, Víctor Campo-Pérez ^{a,b}, Míriam Pérez-Trujillo ^c, Cecilia Cabrera ^d, Jordi Senserrich ^d, Alejandro Sánchez-Chardi ^{e,f}, Rosa Maria Rabanal ^g, Elisabet Gómez-Mora ^d, Estela Noguera-Ortega ^{a*}, Marina Luquin ^a, and Esther Julián ^a

^aDepartament de Genètica i de Microbiologia, Facultat de Biociències, Universitat Autònoma de Barcelona, Bellaterra 08193, Spain; ^bBacterial Infections and Antimicrobial Therapies group, Institute for Bioengineering of Catalonia (IBEC), Barcelona 08028, Spain; ^cServei de Resonància Magnètica Nuclear i Departament de Química, Facultat de Ciències i Biociències, Universitat Autònoma de Barcelona, Bellaterra 08193, Spain; ^dAIDS Research Institute IrsiCaixa, Institut de Recerca en Ciències de la Salut Germans Trias i Universitat Autònoma de Barcelona, Badalona, 08916, Spain; ^eServei de Microscòpia, Universitat Autònoma de Barcelona, Bellaterra 08193, Spain; ^fDepartament de Biologia Evolutiva, Ecologia i Universitat de Barcelona, Barcelona 08028, Spain; ^gUnitat de Patologia Murina i Universitat Autònoma de Barcelona, Bellaterra 08193, Spain

ABSTRACT

The mechanism of action of intravesical *Mycobacterium bovis* BCG immunotherapy treatment for bladder cancer is not completely known, leading to misinterpretation of BCG-unresponsive patients, who have scarce further therapeutic options. BCG is grown under diverse culture conditions worldwide, which can impact the antitumor effect of BCG strains and could be a key parameter of treatment success. Here, BCG and the nonpathogenic *Mycobacterium brumae* were grown in four culture media currently used by research laboratories and BCG manufacturers: Sauton-A60, -G15 and -G60 and Middlebrook 7H10, and used as therapies in the orthotopic murine BC model. Our data reveal that each mycobacterium requires specific culture conditions to induce an effective antitumor response. Since higher survival rates of tumor-bearing mice were achieved using *M. brumae*-A60 and BCG-G15 than the rest of the treatments. *M. brumae*-A60 was the most efficacious among all tested treatments in terms of mouse survival, cytotoxic activity of splenocytes against tumor cells, higher systemic production of IL-17 and IFN- γ , and bladder infiltration of selected immune cells such as ILCs and CD4^{TEM}. BCG-G15 triggered an antitumor activity based on a massive infiltration of immune cells, mainly CD3⁺ (CD4⁺ and CD8⁺) T cells, together with high systemic IFN- γ release. Finally, a reduced variety of lipids was strikingly observed in the outermost layer of *M. brumae*-A60 and BCG-G15 compared to the rest of the cultures, suggesting an influence on the antitumor immune response triggered. These findings contribute to understand how mycobacteria create an adequate niche to help the host subvert immunosuppressive tumor actions.

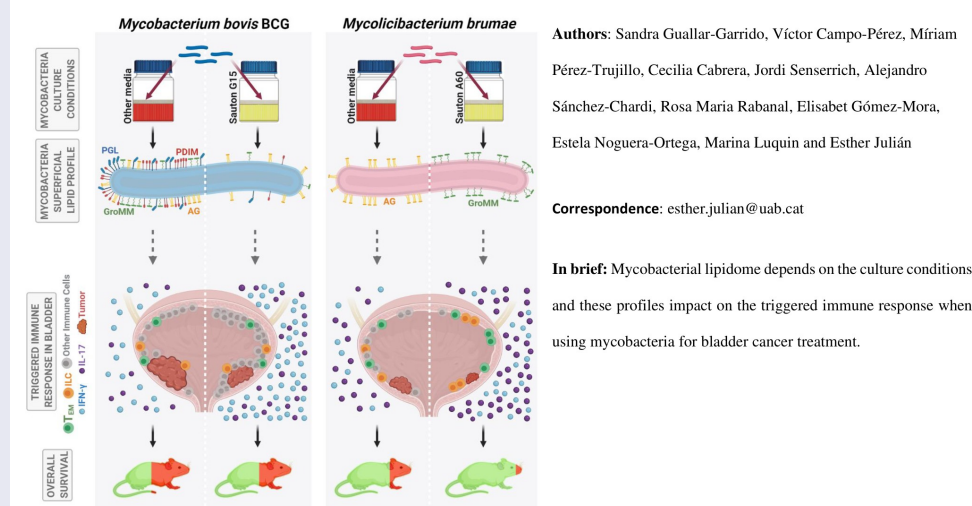
ARTICLE HISTORY



Received 18 October 2021
Revised 7 February 2022
Accepted 7 March 2022

KEYWORDS


Innate-lymphoid cells; innate immune response; non-muscle invasive; BCG; lipid; tumor microenvironment

Mycobacterial surface lipidome remodeled by growth conditions drives the tumor immune microenvironment in bladder cancer treatment



CONTACT Esther Julián  esther.julian@uab.cat  Departament de Genètica i Departament de Genètica i, Universitat Autònoma de Barcelona, Bellaterra 08193, Spain

*Present address: Center for Cellular Immunotherapies and, Division of Pulmonary, Allergy, and Critical Care, Department of Medicine, Perelman School of Medicine, University of Pennsylvania, Philadelphia, PA 19104, USA

 Supplemental data for this article can be accessed on the [publisher's website](#).

© 2022 The Author(s). Published with license by Taylor & Francis Group, LLC.

This is an Open Access article distributed under the terms of the Creative Commons Attribution-NonCommercial License (<http://creativecommons.org/licenses/by-nc/4.0/>), which permits unrestricted non-commercial use, distribution, and reproduction in any medium, provided the original work is properly cited.

Background

High-risk non-muscle invasive bladder cancer (NMIBC) is the most frequent malignant disease in the urothelial tract.¹ The current treatment consists of surgical resection of the tumor followed by weekly intravesical instillations of *Mycobacterium bovis* bacillus Calmette-Guérin (BCG), the tuberculosis vaccine. This treatment is efficacious in more than 70% of patients, preventing recurrence and progression of the disease.² Although BCG treatment is generally well tolerated, both local and systemic complications have led to new research approaches as substitutes for BCG instillations.³ Among these alternatives, nonpathogenic mycobacteria such as *Mycobacterium brumae* have demonstrated antitumor effects. *M. brumae* inhibits bladder tumor cells proliferation at the same time that triggers an antitumor immune response both in *ex vivo* experiments and in the orthotopic murine model of the disease.^{4,5} *M. brumae* have also been demonstrated to be safer than BCG in different animal models.⁶ Snapshots from *in vitro* studies using bladder cancer (BC) cells, *ex vivo* studies using immune cells, and studies of BC patients and orthotopic BC animal models have demonstrated that mycobacteria can interact with both BC cells and immune cells through different mechanisms. The subsequent tumor infiltration by different immune cell populations, ranging from macrophages and granulocytes to effector T cells at the last instillations results in an effective antitumor response. The effect of mycobacteria-induced immunotherapy translates successful treatment of a high percentage of NMIBC patients. However, the effective and precise BCG-induced pathways are still unknown, and they are needed to know whether other mycobacteria can play a major role as a therapeutic treatment.

Many factors have been described as possible reasons for the failure of BCG treatment in almost one-third of treated patients, for instance: the stage of the disease at the time of diagnosis,⁷ the heterogeneity of the tumor,⁸ the genetic background and the immunological status of the patient,^{9,10} and intolerance to BCG instillations.^{11,12} However, very few studies have investigated whether bacterial characteristics themselves influence the success of treatment. BCG is an attenuated species derived originally from pathogenic *Mycobacterium bovis*. Its distribution and maintenance by subculturing in different laboratories worldwide created genetically different substrains with different biochemical characteristics.¹³ The mycobacterial antigenic profile may be crucial when mycobacteria are used for the treatment of NMIBC. These features can differ not only since the existence of several BCG substrains but also because these strains are manufactured under different culture conditions that can affect the antigenic profile. We have recently shown in *in vitro* experiments that cytokine production triggered by BCG or *M. brumae* differs depending on the culture medium in which mycobacteria is grown.¹¹ The impact of culture conditions on BC treatment *in vivo* is unknown, and the antigenic profile that is modified, if any, is also unidentified.

To address how BC immunotherapy treatment is influenced by mycobacteria culture conditions, we studied the antitumor effect triggered by *M. brumae* and BCG grown in four different culture media currently used by research laboratories or manufacturers for BCG production in an orthotopic murine model

of BC. We further analyzed the local and systemic immune response and the lipidome of each mycobacterial strain, enabling us to relate the antigenic profile to the antitumor effect.

Material and methods

Bacterial strains and cell lines

M. brumae (ATCC 51384), and *M. bovis* BCG (Connaught strain) were grown in Middlebrook 7H10 agar (Difco Laboratories, Surrey, UK) supplemented with 10% oleic-albumin-dextrose-catalase enrichment medium for 1 and 4 weeks, respectively. Mycobacteria grown in solid media were used to inoculate bottles with Middlebrook 7H9 medium (Difco Laboratories) supplemented with 10% albumin-dextrose-catalase or different Sauton culture.¹¹ L-asparagine (A) or L-glutamate (G), and different glycerol concentrations (15 or 60 mL/litre) defines the different Sauton media used in this study (A60, G15 and G60). Macroscopic appearance shown in (Supplementary Figure. 1).

The mouse high-grade BC cell line MB49 were maintained in Dulbecco's modified Eagle's medium (DMEM) with stable L-glutamine (Gibco BRL) and supplemented with 10% fetal bovine serum (FBS, Lonza, Basel, Switzerland), containing 100 U/mL penicillin G (Laboratorios ERN, Barcelona, Spain) and 100 g/mL streptomycin (Laboratorio Reig Jofré, Barcelona, Spain), completed media.

Orthotopic model of bladder cancer and intravesical treatment

Animal experiments were approved by the Animal Care Committee at the Autonomous University of Barcelona and executed according to. The orthotopic model of BC in mice was performed following the schedule shown in Figure 1A.⁴ Briefly, 8 and 10 randomized C57Bl/6 female mice (6 to 8-week-old, Charles River Laboratories, Barcelona, Spain) per group were used to study the triggered immune response and survival, respectively.

Animals were maintained in a supine position to perform the experiment. The bladder was emptied and chemical lesions on the urothelium of the bladder were induced by an intravesically instillation of 50 μ L of Poly-L-Lysine solution (PLL, Sigma) through a 24-gauge catheter for 15 min. After pouring out intravesical PLL, tumor was induced to randomized animals by intravesically instilling 100 μ L of DMEM without FBS containing 10^5 MB49 cells. Finally, the bladder was emptied, and animals recovered from the anaesthesia. The day after tumour induction (day 1), mice were anaesthetized and treated with mycobacteria grown in the different culture media. Accordingly, animals received 100 μ L of PBS, 100 μ L of PBS containing 2×10^7 CFU of *M. brumae*, or 100 μ L of PBS containing 2×10^6 CFU of *M. bovis* BCG grown on different culture media. Mycobacteria dose was previously optimized.⁴ Treatments were repeated weekly on day 8, 15 and 22, for

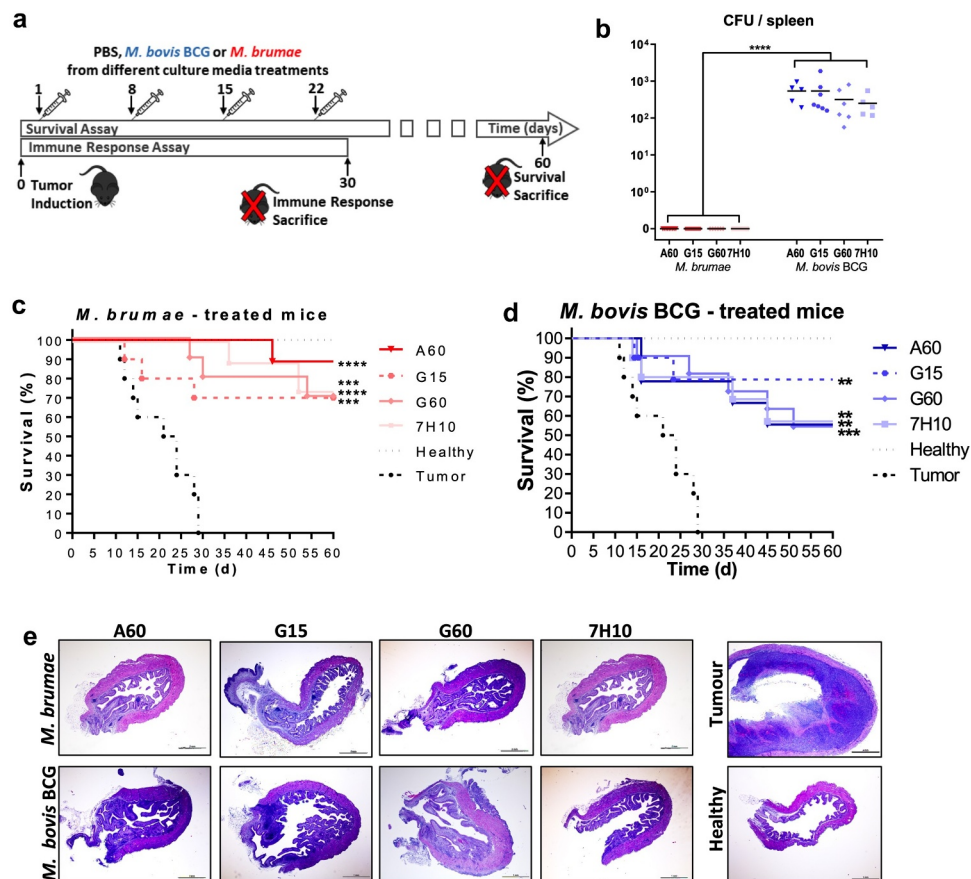


Figure 1. Culture media composition affects the antitumor capacity of mycobacteria. a) Schematic schedule of *in vivo* experiments. Mycobacteria (*M. brumae* and *M. bovis* BCG) pellicles grown in different culture media or PBS were used as treatments for 4 weeks, after tumor induction in female C57Bl/6 mice. In a first set of experiments, survival rates were evaluated 60 days after tumor induction (N = 10). In a second set of experiments the triggered immune response in tumor-bearing mice was studied 30 days after tumor induction (N = 8). b) Colony-forming units (CFU) of spleens from *M. brumae*- (red) and *M. bovis* BCG- (blue) treated mice. Mycobacteria counts from each spleen is represented by a dot; the line identifies the median for each group. **p* < 0.05 Kruskal–Wallis test, Dunn’s multiple comparison test. c–d) Kaplan–Meier analysis of healthy and tumor-bearing mice survival after PBS or *M. brumae* or *M. bovis* BCG treatments. **p* < 0.05 versus PBS group, log-Rank (Mantel-Cox) test. e) Representative histological images (hematoxylin-eosin staining) of bladder sections from non-treated (PBS), *M. brumae*- and *M. bovis* BCG-treated tumor-bearing mice. Scale refers to 1 mm. A60 is L-asparagine plus 60 mL of glycerol per L of medium; G15 is L-glutamate plus 15 mL/L of glycerol; G60 is L-glutamate plus 60 mL/L of glycerol; 7H10 is Middlebrook 7H10 medium.

a total of 4 treatments. A negative (healthy mice) and a positive (non-treated tumour-bearing mice) control group were used in all the experiments. Healthy mice received the PLL instillation, but PBS was used instead of either BC tumour cells or mycobacteria treatments. Non-treated tumour-bearing mice received PLL and BC tumour cells, but PBS was used for the intravesical treatments.

Mycobacteria suspension was prepared as previously reported.¹¹ Briefly, mycobacteria from pellicles were recovered using a sterile KÖlle handle, dried under the hood and transferred to a sterile glass tube containing 3 mL of phosphate-buffered saline (PBS) and glass beads to disaggregate mycobacteria clumps. Then, supernatant was adjusted to McFarland 1 and centrifuged at 1640 *g* for 10 min. Pelleted bacteria were resuspended in PBS to achieve the final concentration. Inoculums were corroborated by plating the solution in 7H10 Middlebrook plates. CFU/mL were obtained after incubating *M. bovis* BCG plates at 37°C for three weeks and *M. brumae* plates for one week.

All experiments were carried out under inhaled anaesthesia, 1.5–2% isoflurane in pure O₂ and eyes protected with liquid ophthalmic gel. Tumour implantation was ensured from day 7 to 10 due to the presence of blood in urine. During the

experiment, all animals were housed with a maximum of six animals per cage with food and water *ad libitum* in an enriched environment, in a Biosafety Level (BSL) 2 facility. Animal behavior and well-being were evaluated daily to avoid unnecessary suffering and animals were euthanized when it was required. To analyze the immune response, animals were sacrificed at day 30, blood was collected by cardiac puncture and spleens and bladders removed in aseptic conditions. In survival analyses, surviving animals were sacrificed at day 60, and bladders and spleens were collected in aseptic conditions and processed for histopathological evaluation and CFU counting.⁴ For histopathologic analyses, bladders were collected and immediately fixed in formaldehyde 4%. Then, hematoxylin-eosin staining was performed in 2–3 μ m-sections of embedded bladders in paraffin. Representative images were obtained from all conditions for histopathologic analyses.

Restimulation and cytotoxic capacity of splenocytes

Spleens were disrupted with tweezers. Homogenized splenocytes diluted in DMEM complete media were added on 96-well tissue culture plates (Thermo Scientific) containing 10⁵ MB49 cells (25:1,

splenocyte:tumor cell). After incubation for 24 h at 37°C containing 5% of CO₂, wells were vigorously washed with warm PBS and MTT was performed to measure MB49 cells viability.⁴ Splenocytes adjusted to a final concentration of 3×10^6 cell/mL were also seeded to evaluate proliferation upon restimulation. Accordingly, 180 µL of splenocyte suspension was restimulated with 1 mg/mL of heat-killed mycobacteria grown in each medium within 20 µL. PBS was used as negative control, and 5 µg/mL of Concanavalin A (ConA, Sigma) as positive control. After 72 hours of incubation plates were centrifuged, supernatants collected and MTT assay performed in pelleted splenocytes.

IFN- γ , Interleukin (IL)-4 and IL-17 cytokines were measured in supernatants by using commercially available ELISA tests (Mabtech AB, Nacka Strand, Sweden).

IgG antibody detection in sera

Blood was centrifuged and sera frozen until use. To analyze the presence of total IgG in sera, the bottom of 96-well plate wells was coated with 20 µg/mL of heat-killed-*M. brumae* or heat-killed-BCG, grown in the different media. ELISA procedure was performed as described before.⁵ Blank wells consist on sera without antigen and its absorbance was deducted to wells with sera and antigen for each animal.

Detection of infiltrated immune cell subsets into the bladders

The immune infiltrate present into the bladder was analyzed by flow cytometry as previously described.⁵ Briefly, bladders were minced using a scalpel followed by digestion with RPMI medium supplemented with 5% FBS containing 0.5 mg/mL collagenase II (Sigma, Spain) and 1 U/mL DNase I at 37°C for two-three successive 30 min cycles, with continuous shaking. The cell suspension obtained was filtered through a 40-µm disposable plastic strainer (Becton & Dickinson) and pelleted for staining. The cells were labeled with the following antibodies: PerCP-CD45 APC-Cy7-CD3, FITC-CD4, Alexa 700-CD8, APC-CD62L and BV786-CD127, PE-Dazzle-CD44 and FITC-CD45R/B220 (Biolegend). The lymphocyte gate was defined by morphological parameters, and dead cells were excluded using a live/dead fixable Aqua Dead Cell Stain kit (Invitrogen). Samples were acquired in a Fortessa flow cytometer (Becton & Dickinson), and the data were analyzed using FlowJo software (9.8 v; TreeStar, Portland, OR, USA). Absolute cell numbers were obtained by using Perfect-Count Microspheres (Cytognos). Gating strategy is shown in Supplementary Figure 3.

Superficial and total lipid extraction of pellicles

After properly growth of four independent cultures of each strain in each culture media, lipids from the surface of the mycobacteria pellicles were extracted with petroleum ether (PE) (40–60°C b.p.) for 5 min.¹⁴ PE extracts were dried under nitrogen stream and analyzed by thin layer chromatography (TLC) on silica gel-coated plates (G-60, Merck, Germany).

To analyze the total mycobacterial lipidic composition, cells recovered from four independent cultures of each strain in each culture medium were exposed to chloroform/methanol suspensions as described before.¹⁵ Lipidic extracts were analysed by thin-layer chromatography (TLC) on silica gel-coated plates (G-60, Merck, Germany) using chloroform/methanol (96:4, v/v) or PE (60–80°C b.p.)/diethyl ether (90:10, v/v). TLC were revealed by using phosphomolybdic acid (VWR, USA; 10% in ethanol) followed by heating the plate at 120°C. One representative TLC for each condition is shown in the Results section.

Lipid purification and analysis

Purification of spots 1, 2, 3 and 4 from two independent lipidic extracts was performed as previously described with slightly modifications.¹⁶ Briefly, lipid extract resuspended in chloroform was added to a Silica Gel 60 (Merck, Germany) column stabilized with PE (60–80°C b.p). Increasing diethyl ether concentrations were used for spots elution. Fractions containing the eluted spots were dried and used for nuclear magnetic resonance (NMR) analyses. Purification of spots A, B and C were done as 1, 2, 3 and 4 spots, yet using chloroform to stabilize the column and increasing methanol concentrations to elucidate the spots.

For the NMR analysis each purified compound was dissolved in 600 µL of CDCl₃ (99.80% D, Cortecnet, Voisins-le-Bretonneux, France). A Bruker Avance II 600 NMR spectrometer (Bruker Biospin, Rheinstetten, Germany) equipped with a 5 mm TBI probe operating at a ¹H and ¹³C NMR frequencies of 600.13 and 150.90 MHz, respectively, was used. All experiments were performed at 298.0 K. 1D ¹H NMR spectra were acquired using a standard 90° pulse sequence, with an acquisition time of 1.71 s and a relaxation delay of 2 s. Data were collected into 32 K computer data points, with a spectral width of 9590 Hz and as the sum of 1024 transients. In the case of quantitative 1D ¹H NMR spectrum the relaxation delay was set to 15s. 2D NMR experiments ¹H,¹H-COSY (Correlation Spectroscopy) and ¹H,¹³C-HSQC (Heteronuclear Single Quantum Coherence) were performed using standard Bruker pulse sequences and acquired under routine conditions. All spectra were calibrated using the residual solvent signal (CHCl₃, δ_H , 7.26 and δ_C , 77.0 ppm). Multiplicity of peaks is abbreviated as s (singlet), d (doublet), t (triplet), dd (doublet of doublets) and m (multiplet). Integration was performed with the global spectral deconvolution (GSD) application of MestreNova 8 (Mestrelab Research S.L.).

Ultrastructure of pellicles

Grown pellicles were collected with nucleopore membrane (Whatman® Nuclepore™) and placed in aluminum foil structures incorporated into 6-well plates (Nunc® Thermo Scientific™). Then, pellicles were fixed with osmium vapors by adding 250 µL/well of 4% osmium tetroxide (TAAB Lab., UK) and maintained at 4°C overnight. Fixed biofilms were air dried, placed on stubs and coated with Au-Pd (Emitech Au-Metallizer). Pellicle ultrastructure was observed with a secondary electron detector in a SEM EVO® MA 10 (Zeiss, Oberkochen, Germany) operating at 15 kV.

Neutral red staining of mycobacteria

Neutral red staining was performed as previously reported with few modifications.¹⁷ Briefly, mycobacteria pellicles were filtered, completely dried under hood, and transferred to a screw-cap tube containing 5 mL of 50% methanol in deionized water. Then, cells were mixed and incubated for 1 h at 37°C. Washing process was repeated twice. Finally, mycobacteria were mixed with 2 mL of 0.002% neutral red (Merck, Germany) in barbital buffer (1% sodium barbital in 5% NaCl [pH 9.8]) and incubated at room temperature. Results were obtained 1 hour later.

Statistical analysis

Graphpad Prism 6.0 software (San Diego, CA, USA) was used for statistical analyses. Log-rank (Mantel-Cox) test was used to evaluate differences between mice survival curves. *Ex vivo* experiments were analyzed using ANOVA. Quantitative data are expressed as the mean \pm standard deviation ($\bar{x} \pm SD$). Immune infiltration data were analyzed using Mann-Whitney tests, and their correlations to IL-17 and IFN- γ were analyzed by Spearman tests. Statistical significance was assumed at $p < 0.05$.

Results

Tumor-bearing mouse survival rates depend on mycobacterial culture medium composition

The antitumor effect of mycobacteria grown in different culture media was studied in the orthotopic murine model of BC (schedule shown in Figure 1A). Mycobacteria-treated tumor-bearing mice survived statistically longer than untreated mice, with survival rates higher for *M. brumae*-treated mice than for BCG-treated mice, in agreement with previous studies⁴ (Figure 1C-D). Notably, *M. brumae* grown in A60 culture medium (*M. brumae*-A60) prolonged survival in 100% of mice 40 days after tumor induction and in 89% of mice at the end of the experiment, being superior to the rest of *M. brumae* treatments (Figure 1C and Supplementary Table 1 and Table 2), although without statistical significance. For BCG treatments, 70% of mice treated with BCG grown in G15 (BCG-G15) survived until the end of the study, the most successful treatment among all BCG treatment regimens (Figure 1D and Supplementary Table 1 and Table 2). Histological examination of the urinary bladder showed mild to moderate lymphoplasmacytic infiltrates in the lamina propria, with lymphoid follicle formation near the neck of the bladder, in most mycobacteria-treated mice. The lymphocytic infiltrates were slightly more intense in BCG-treated mice (Figure 1E).

Pathogenicity was not influenced by culture media, being BCG present in spleens from BCG-treated mice, and *M. brumae* absent in *M. brumae*-treated mice, corroborating its non-pathogenicity^{4,6} (Figure 1B).

Culture medium composition influences the mycobacteria-triggered systemic immune response

Restimulated splenocytes from *M. brumae*-A60- and BCG-G15-treated mice showed the highest proliferation ratios, which were significantly higher than those observed for

the rest of the conditions (Figure 2A). Regarding cytokine production, a massive IFN- γ release triggered by BCG treatments compared to all *M. brumae* treatments (one log inferior) was observed (Figure 2B), with *M. bovis* BCG-G15-treated mice having the highest IFN- γ production. Splenocytes from *M. brumae*-A60-treated mice exhibited more IFN- γ release than those from the other tested conditions, with a significant difference between *M. brumae*-G60- and *M. brumae*-7H10-treated mice. In contrast to IFN- γ , IL-17 was overproduced in splenocytes from *M. brumae*-treated mice compared to those from BCG-treated mice. Specifically, IL-17 levels in splenocyte cultures from *M. brumae*-A60-treated mice were superior to those in splenocyte cultures from *M. brumae*-G15-, *M. brumae*-G60- or *M. brumae*-7H10-treated mice (Figure 2B). Although no significantly different, splenocytes from BCG-G15-treated mice showed slightly higher levels than those from the other BCG-treated mice (Figure 2B). IL-4 was not detected in any condition (data not shown).

When splenocytes from A60-, G15- or G60-treated mice were restimulated with mycobacteria grown in 7H10, proliferation ratios were lower than those obtained in splenocytes restimulated with mycobacteria grown in the same medium used for intravesical treatment (Supplementary Figure. 2A). These results indicate specificity in reactivity against mycobacterial antigens produced in each culture medium. Both the proliferation ratios and IL-17 production obtained in *M. brumae*-A60- and BCG-G15-treated mice again showed the highest values (Supplementary Figure. 2A and 2B).

When cytotoxicity was studied, splenocytes from *M. brumae*-A60-treated mice showed the highest growth inhibition of MB49 cells (reducing up to 30% of cell growth) compared to splenocytes from the rest of the groups (Figure 2C). Likewise, splenocytes from the other groups of *M. brumae*- and BCG-treated mice had similar cytotoxic effects on MB49 cells (Figure 2C).

No significant differences in anti-mycobacterial antibodies in the serum were detected among treatments, but higher production of IgG was detected in *M. brumae*-treated mice than in BCG-treated mice when mycobacteria were grown in Sauton media (Figure 2D), contrary to the results obtained when mycobacteria were grown in 7H10 (Figure 2D and^[5]). When cross-reactivity was analyzed, IgG levels from serum of *M. brumae*-7H10-treated mice were higher than those produced against *M. brumae* grown in the culture medium used for intravesical treatment (Supplementary Figure. 2C). In all cases, *M. brumae*-treated mice showed higher antibody levels than BCG-treated mice.

Bladder immune cell infiltration differs between BCG and *M. brumae* treatments

All mycobacterial treatments induced robust infiltration of different populations of lymphocytes (CD45⁺, CD3⁺, CD4⁺ and CD8⁺ T cells, NK cells and B cells) into the bladder compared to no treatment (Figure 3A). Statistical differences among groups are shown in Supplementary Table 3. When comparing both mycobacterial treatments, mice receiving BCG

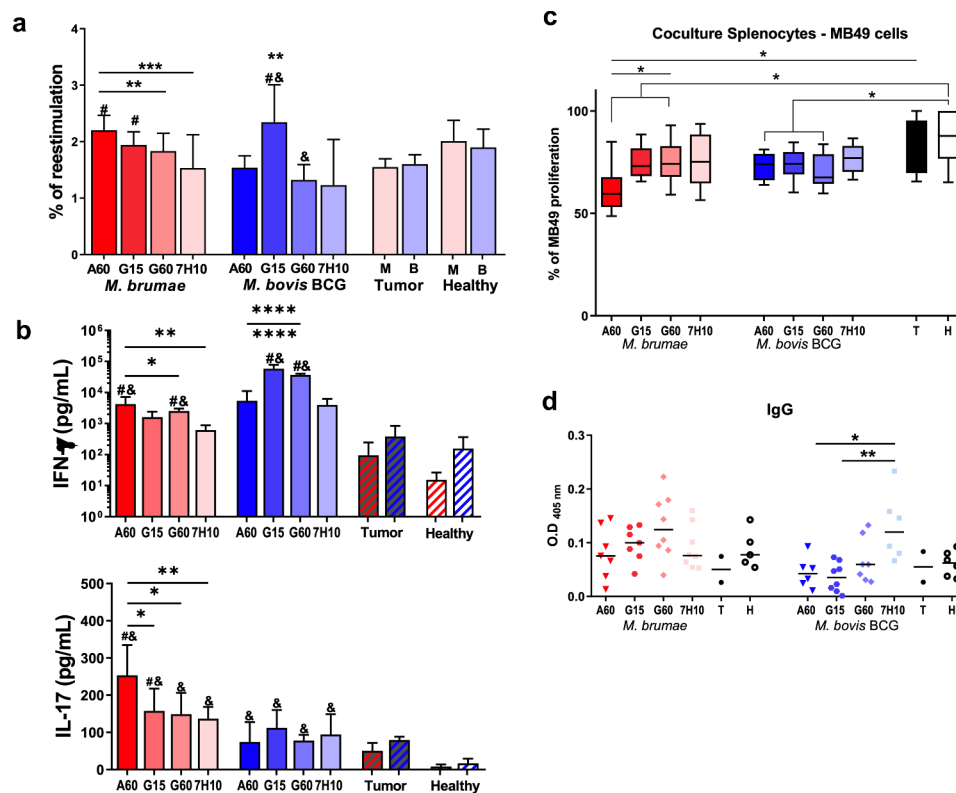


Figure 2. Different systemic immune response triggered by mycobacteria. a) Percentage of proliferation of mycobacteria-restimulated splenocytes over non-stimulated splenocytes from mycobacteria-treated tumor-bearing mice; and b) IFN- γ and IL-17 cytokine detection in culture supernatants from restimulated splenocytes. Splenocytes were restimulated with heat-killed *M. brumae* (red) or BCG (blue) grown in the same medium used for intravesical treatment; c) MB49 cell inhibition triggered by splenocytes from *M. brumae*- (red), BCG- (blue), and non-treated (grey) tumor-bearing mice, and healthy (white) mice. Ratio 25:1 (splenocytes:MB49 cells). d) Anti-*M. brumae* (red) or anti-BCG (blue) IgG antibodies detected in sera from mycobacteria-treated mice. T is non-treated tumor-bearing mice; H is healthy mice. Data represents the mean and SD. * $p < 0.05$, # $p < 0.05$ with respect to tumor, and & $p < 0.05$ with respect to healthy mice (ANOVA test).

had significantly higher absolute immune infiltration of total CD45⁺ cells and T, NK and B cells than *M. brumae*-treated animals (Figure 3A). Differences were also observed when comparing the effects of culturing each mycobacterial strain in different media. Among all conditions, mycobacteria grown in G15 induced the highest infiltration levels, while mycobacteria grown in A60 induced the lowest infiltration levels. Statistical significance was only reached between animals treated with BCG grown in G15 and A60 for the total numbers of CD45⁺ lymphocytes and CD4⁺ T cells, with a trend for the number of infiltrating CD3⁺ T cells (Figure 3A). In *M. brumae*-treated mice, B cell numbers were also significantly increased in G15 culture conditions compared to the other culture conditions, and a trend toward differences in NK cell infiltration was also found when comparing G15 and A60 media (Figure 3A). Remarkably, the amount of IFN- γ secreted by splenocytes from treated mice restimulated with mycobacteria showed strong correlations with the frequencies of CD3⁺, CD4⁺, and CD8⁺ T cells and CD4⁺ effector memory T (T_{EM}) cells within bladder tumors (Figure 3B).

As *M. brumae* treatment induced high IL-17 production by splenocytes upon restimulation (Figure 2B), we sought to identify whether there is a link between systemic immune response and local immune infiltration. Frequencies of innate lymphoid cells (ILCs, defined as CD3⁻CD127⁺ cells) and CD4⁺ T_{EM} cells in the bladder robustly correlated with the levels of this cytokine produced

by splenocytes (Figure 3C). Remarkably, these correlations were observed when analyzing only *M. brumae*-treated mice, not BCG-treated mice. Both populations were enriched in bladders from *M. brumae*-A60-treated tumor-bearing mice in comparison to mice given any other treatment, although the differences only reached statistical significance for CD4⁺ T_{EM} cells (Figure 3D). Interestingly, although BCG treatment induced stronger tumor immune cell infiltration than *M. brumae* treatment, the frequency of ILCs was significantly higher in *M. brumae*-treated animals than in BCG-treated animals. In contrast, we did not observe differences in the proportion of CD4⁺ T_{EM} cells between BCG- and *M. brumae*-treated mice when the results for each mycobacteria strain, regardless of culture medium, were pooled together (Figure 3D).

Culture medium composition modifies the mycobacterial cell-surface lipidomic profile

The ultrastructural appearance of the outermost layer deciphered a thin layer covering all bacilli, although growing in the different culture media (Figure 4A and 5A). However, while *M. brumae* appears as a prearranged mass in which individual cells can be clearly observed, BCG cultures showed an extracellular matrix covering the cells, as previously reported.¹¹

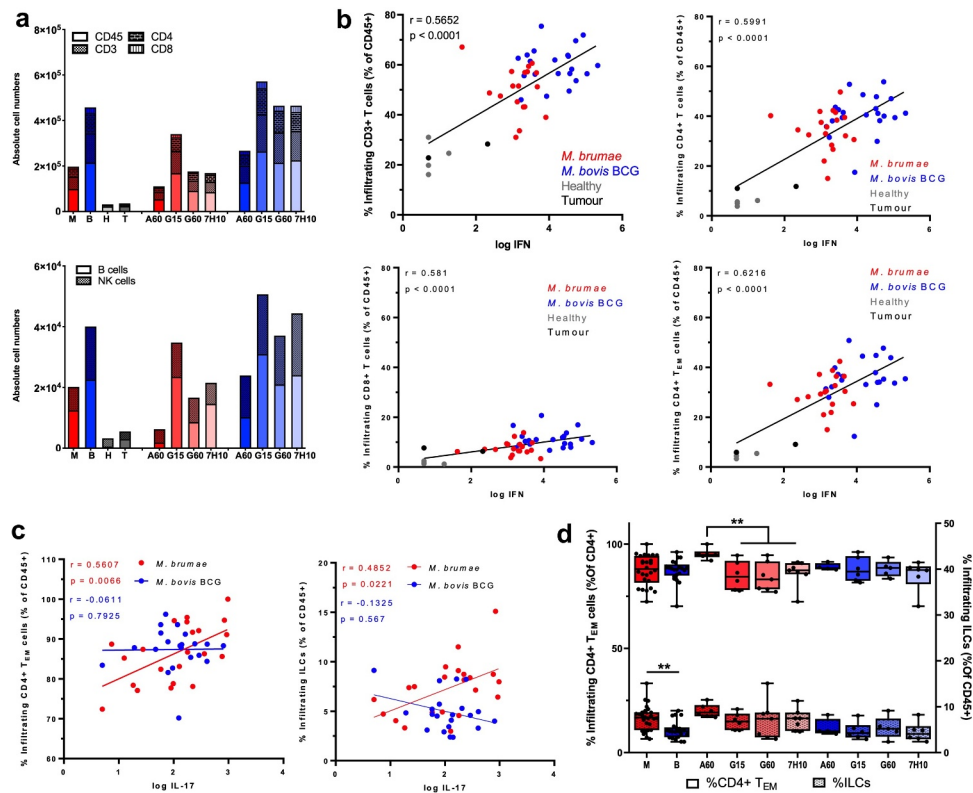


Figure 3. Mycobacteria systemic effects are linked to local bladder tumor immune features. a) Immune infiltration in the bladder of healthy mice (H), untreated tumor-bearing mice (T) and mycobacteria-treated tumor-bearing mice, either BCG (B) or *M. brumae* (M) grown in different media. Absolute numbers of infiltrating CD45⁺, CD3⁺, CD4⁺ and CD8⁺ T cells (top graph) and B and NK cells (bottom graph) are given. b) Positive correlation between CD3⁺, CD4⁺, CD8⁺ T and CD4⁺ effector memory (T_{EM}) cell frequencies and the levels of IFN- γ produced by re-stimulated splenocytes. Each dot represents one mouse (*M. brumae* in red; BCG in blue; healthy in light grey; untreated tumor in dark grey). Pearson *r* and *p* values are shown. c) Secretion of IL-17 by re-stimulated splenocytes significantly correlates to the frequency of CD4⁺ T_{EM} cells and innate lymphoid cells (ILCs) in *M. brumae*-treated mice (*M. brumae* in red; BCG in blue). Pearson *r* and *p* values are indicated. d) Frequency of CD4⁺ T_{EM} cells and ILCs infiltrating bladder tissue from healthy or tumor-bearing mice, treated with BCG or *M. brumae* grown in different culture media. Mean \pm SD values are given, with dots representing individual mice. ***p* < 0.01.

Then, the lipidic composition of the superficial layer of mycobacteria was obtained by a short extraction with PE and analyzed by TLC and NMR spectroscopy. Eluting the TLC products with chloroform/methanol (96:4, v/v), spot A was only detected in *M. brumae*-A60 and *M. brumae*-G60 (Figure 4B). The ¹H NMR spectrum of spot A was in accordance with that of glycerol monomycolate (GroMM) structures,¹⁸ with the mycolate unit being an α -mycolic acid (Figure 4D). Confirmation of this molecule was achieved by the performance of 1D and 2D NMR experiments (1D ¹H, ¹H-¹H COSY and ¹H-¹³C HSQC), which allowed complete ¹H and ¹³C NMR characterization of the molecule (Supplementary Table 4). Resonances of the glycerol mono-substituted unit were identified as H1a and H1b at 4.28 and 4.24 ppm, respectively, H2 at 3.96 ppm, and H3a and H3b resonated at 3.75 and 3.63 ppm, respectively. The typical peaks of α -mycolates were identified and were in accordance with published studies.¹⁹ Among them, olefinic protons of *trans* double bonds (multiplets at 5.33 and 5.24 ppm from H10 and H11, respectively) and *cis* double bonds (multiplet at 5.35 ppm from H9) were shown. Finally, peak integrations were in accordance with the structure of α -GroMM. To determine the specific diastereoisomers of α -GroMM of spot A, a more detailed analysis of H1a and H1b was carried out. The 1D ¹H spectrum

showed a slightly different H1a and H1b signal pattern compared to that shown before.¹⁸ These differences could be due to a change in the solvent used and/or to differences in the global structure of the molecule (since previous GroMM molecule analysed contains a different mycolate). However, in the present study, α -GroMM also showed two different H1b signals, indicated as H1b (dd at 4.242 ppm) and H1b' (dd at 4.228 ppm), which are partially overlapped (Supplementary Figure 4 and Supplementary Table 4). Additionally, the relative integration of H1a and (H1b + H1b') signals was 1.00 to 1.03. This evidence suggested the presence of a mixture of the *R* and *S* diastereoisomers

Eluting the TLC products with PE/diethyl ether (90:10, v/v), spots 1, 2, 3, and 4 were observed in *M. brumae* grown in all cultures except in the A60 culture. According to NMR analyses, spot 1 was identified as having molecular structures containing long aliphatic chains and aromatic groups (Supplementary Figure 5), spot 2 was identified as having molecules containing long chains with *cis* and *trans* insaturations (Supplementary Figure 6), and spots 3 and 4 were identified as acylglycerides (AGs). Nevertheless, all culture conditions permitted the accumulation of AG in deeper layers of the cell wall or the cytoplasm since a total lipidic extraction of *M. brumae* clearly showed a spot corresponding to AG (Figure 4C), even in the case

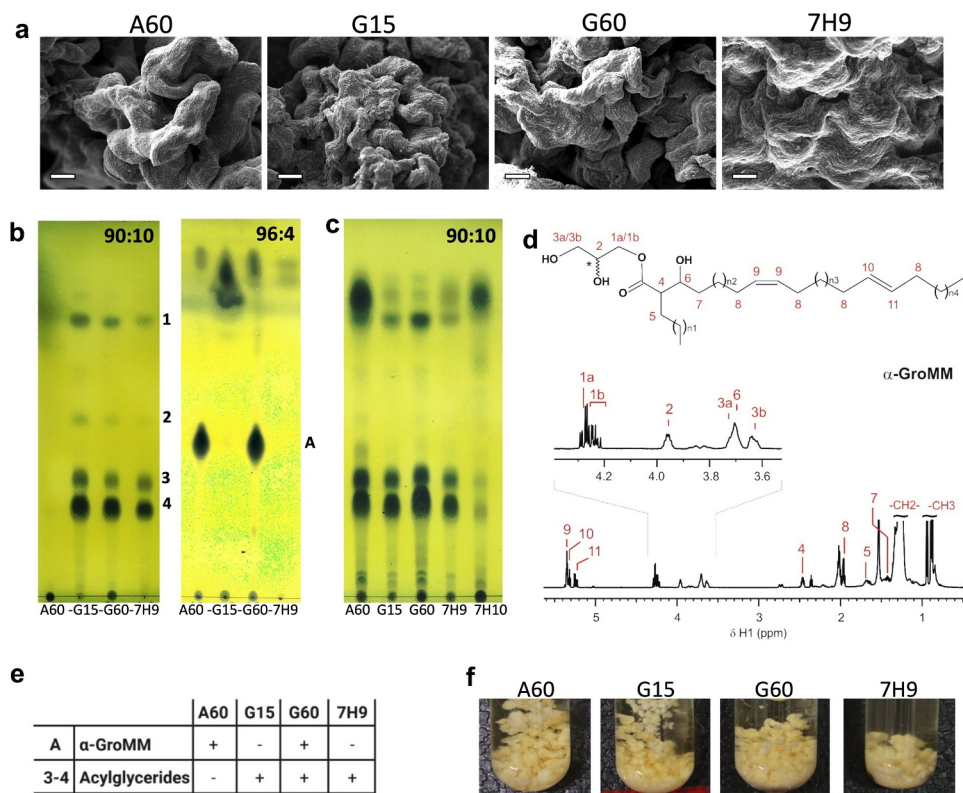


Figure 4. Superficial lipid analyses of *M. brumae*. a) SEM representative micrographs of *M. brumae* grown in the four culture media, bars size are 40 μm; b and c) Thin layer chromatographies (TLC) corresponding to the superficial lipids (b) and total lipids (c) of *M. brumae* pellicles grown on different culture media. The volume of lipid extracts applied to TLC plates was equal in all culture conditions and derived from the same amount of lipid extractions in the surface of the pellicles. The results are one representative experiment out of at least four biological replicates. TLC plates were eluted in chloroform-methanol at 96:4 (v/v), or PE 60–80°C -diethyl ether at 90:10 (v/v). TLC plates were revealed with 10% phosphomolybdic acid in ethanol; d) ¹H NMR spectra of purified α-GroMM. CDCl₃ was used as solvent and spectra were acquired at a magnetic field of 600 MHz and at a temperature of 298.0 K; e) summarized tables of the superficial lipids obtained from *M. brumae* pellicles; f) images corresponding to the neutral red staining in *M. brumae* cells. α-GroMM, alpha-glycerol-monomycolates; AG, acylglycerol.

of *M. brumae*-A60, in which AG was absent on the outermost cell surface. Similar lipidic profiles in G15-, G60- or 7H9-*M. brumae* were observed (Figure 4B).

Notable differences were observed among lipid extracts from BCG pellicles grown in different culture media (Figure 5B and 5C). In the A60 and G60 cultures, two spots (B and C) were highly expressed, while both spots were less produced by BCG grown in medium with a low glycerol concentration (G15). Remarkably, only spot C was detected in BCG-7H9 (Figure 5B). Spot B and spot C of BCG were identified and fully characterized using 1D and 2D NMR spectroscopy. Spot B corresponded to phenol glycolipid (PGL) (Supplementary Figure 7 and Supplementary Table 5),²⁰ whereas spot C corresponded to a GroMM structure formed mainly by keto-mycolates (k-GroMM, Figure 5D).¹⁸ For spot C, the NMR resonances of the monosubstituted glycerol unit of k-GroMM coincided with those described before for α-GroMM and typical peaks of the keto group and *cis* cyclopropane appeared (Figure 5D, Supplementary Figure 8 and Table 4). The integration of signals in a quantitative 1D ¹H NMR spectrum showed that the GroMM molecular structure in spot C was mainly formed by keto-mycolates in form of a mixture of *R* and *S* diastereoisomers (Supplementary Figure 4).

Moreover, less PGL and almost untraceable phthiocerol dimycocerosate (PDIM) levels were detected on the surface of BCG-G15 pellicles in comparison with the other BCG conditions (Figure 5B). The analysis of the total lipid extract corroborated a diminished production of PGL, PDIM and GroMM by BCG-G15 cultures (Figure 5C). Finally, the physicochemical properties of mycobacteria were studied by neutral red staining of cells. BCG-A60, BCG-G60 and BCG-7H10 cells showed a distinctive strong pink color but not the intense deep red color produced by *Mycobacterium tuberculosis* pathogenic strains.²¹ This result indicates the presence of mycobacterial compounds with reducing power, suggesting different physicochemical characters of the cell wall in all *M. brumae* conditions and BCG-G15 cells (Figures 4F and 5E).

Discussion

Our results indicate that mycobacteria grown in different culture media trigger different antitumor activities in an orthotopic murine model of BC. Furthermore, each mycobacterial strain requires specific culture conditions to induce an effective antitumor response since higher survival rates of tumor-bearing mice were achieved using BCG-G15 and *M. brumae*-

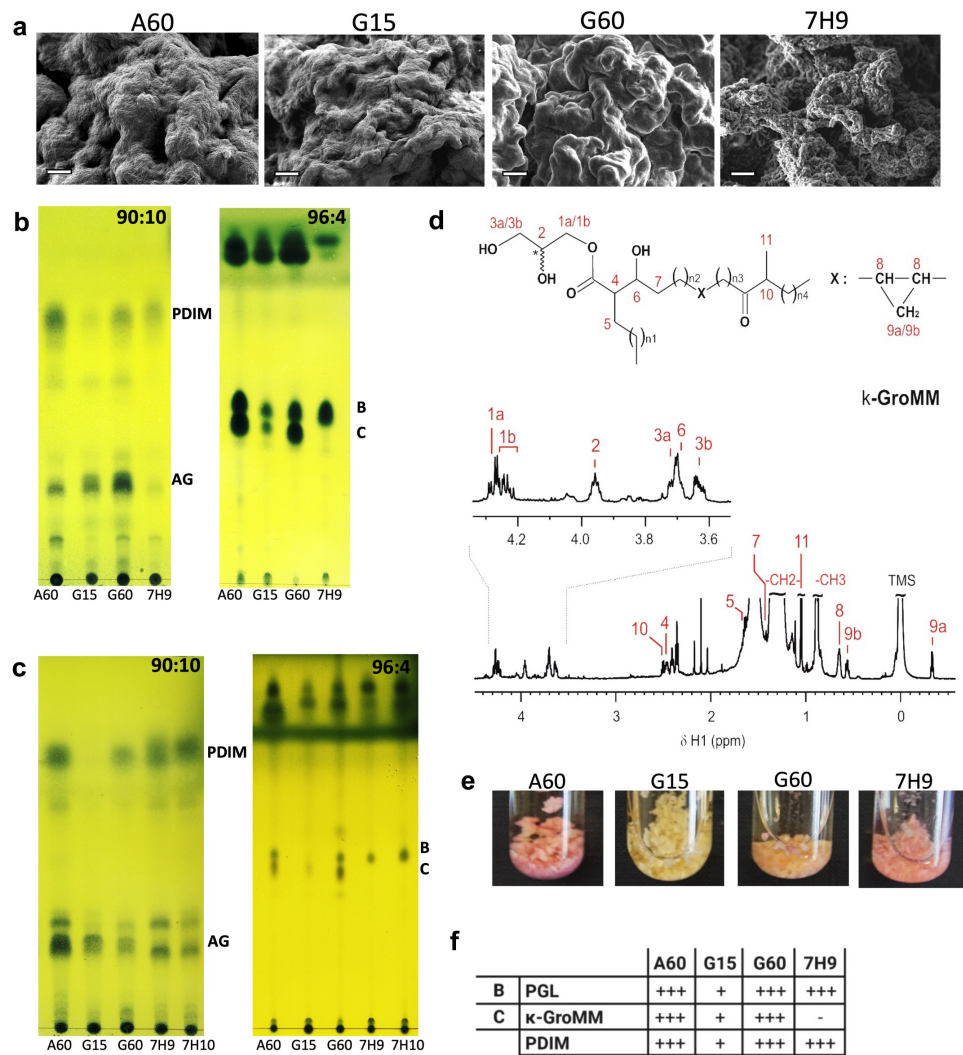


Figure 5. Superficial lipid analyses of *M. bovis* BCG. a) SEM representative micrographs of *M. bovis* BCG grown in the four media, bars size are 40 μ m; b and c) Thin layer chromatographies (TLC) corresponding to the superficial lipids (b) and total lipids (c) of BCG pellicles. The volume of lipid extracts applied to TLC plates was equal in all culture conditions and derived from the same amount of lipid extractions in the surface of the pellicles. The results are one representative experiment out of at least four biological replicates. TLC analyses were eluted in chloroform-methanol at 96:4 (v/v), or PE 60–80°C -diethyl ether at 90:10 (v/v). TLC plates were revealed with 10% phosphomolybdic acid in ethanol; d) ^1H NMR spectra of purified κ -GroMM. CDCl_3 was used as solvent and spectra were acquired at a magnetic field of 600 MHz and at a temperature of 298.0 K; e) images corresponding to the neutral red staining in BCG cells; (f) summarized tables of the superficial lipids obtained from BCG pellicles. κ -GroMM, keto-glycerol-monomycolates; PGL, phenolic glycolipid; AG, acylglycerol, PDIM, phthiocerol dimycocerosates.

A60 than the rest of the treatments. The inhibition of bladder tumor growth was accompanied by local and systemic immune responses that also differed between the two species. Outstandingly, *M. brumae*-A60 was the most efficacious among all tested treatments in terms of mouse survival and cytotoxic activity of splenocytes against tumor cells. Therefore, comparing *M. brumae*-A60 with BCG treatments provides the possibility to unravel traits of the mechanisms involved in the antitumor activity of mycobacteria *in vivo*.

After the evaluation of the systemic immune activation, we observed that *M. brumae*-A60 and BCG-G15 triggered the highest IL-17 and IFN- γ production, respectively, which was significantly different from that triggered by the rest of the treatments. The role of the cytokine IL-17 in cancer immunotherapy is under discussion, as its function can vary depending on the type of cancer. In BC, high levels of IL-17 in BCG-treated patients have been related to high survival rates. IL-17 upregulates IL-8 and IL-6 expression,

directly inhibiting BC cells²² and inducing higher infiltration of neutrophils into the bladder after BCG instillation.²³ In *M. brumae*-treated mice but not in BCG-treated mice the production of IL-17 correlates positively with the presence of CD127⁺ ILCs in the bladder, whose infiltration is significantly increased, especially in *M. brumae*-A60-treated mice.

ILCs include cytotoxic natural killer (NK) cells and cytokine-producing ILCs (helper-like ILC types 1, 2 and 3), which are considered the innate homologs of Th1, Th2 and Th17 responses^{24,25} and display features of mature effector lymphocytes. Considering the positive correlation between IL-17 production and the presence of ILCs, the presence of type 3 ILCs, which produce IL-17 after stimulation, is plausible in *M. brumae*-treated mice. The roles of these subsets in shaping anti-tumor immunity are the focus of intense study.^{26–29} In the case of BC, Chevalier *et al.* analyzed the immune cell distribution in the urine of NMIBC patients during BCG treatment, and ILC2s

were found to be the most abundant innate lymphoid cell subpopulation present in patients with BCG treatment failure.³⁰ The same authors demonstrated that CCR4 may be involved in the recruitment of ILCs in the bladder during BCG therapy.³⁰ Thus, ILCs are stimulated after mycobacterial treatment, and each type of ILC could play a distinct role in BC outcomes. Interestingly, transcriptome cross-species analysis showed similarities between mouse ILC1 and ex-ILC3 subsets and human CD56^{bright} NK cells,³¹ which have a relevant role in BC patients treated with BCG.³² Hence, understanding how and which of these subsets are regulated after *M. brumae* or BCG instillation in BC might yield significant insights into the mechanisms of mycobacteria-based therapy.

CD4 T_{EM} cells are another immune cell population able to produce IL-17, which positively correlates with *M. brumae*-treated mice, in contrast to the negative correlation found in BCG-treated mice. In the case of BCG, CD4 T_{EM} cells were only positively correlated with IFN- γ production. In the case of *M. brumae*-A60, the IL-17 response was accompanied by significant production of IFN- γ compared to the rest of the *M. brumae* treatments. The role of mycobacteria-triggered IFN- γ production via the Th1 response has been widely described in the resolution of BC.^{13,30,33} Early works showed the relevance of the recruitment of CD4 and CD8 T cells to resolve bladder tumors in animal models, and even recombinant BCG expressing Th1 cytokines and combinations of BCG therapy plus cytokine addition are currently under study to overcome BCG unresponsiveness in BC patients.^{34,35} Remarkably, BCG-G15 treatment triggered the highest systemic IFN- γ production and massive bladder infiltration of immune cells, mainly CD3⁺ (CD4⁺ and CD8⁺) T cells, observed by both flow cytometry and histological analysis. Overall, systemic IL-17 and IFN- γ production together with immune cell infiltration into the bladder indicates that while BCG-G15 antitumor activity could be based on massive infiltration together with high IFN- γ release (high systemic and local inflammation), *M. brumae*-A60 could be more effective in inducing the infiltration of selected immune cells, mainly IL-17 producers, which could create an adequate niche to help the host subvert immunosuppressive tumor actions.^{33,36}

Reasonably, the first interaction between intravesically instilled mycobacteria and BC or innate immune host cells could be the determinant for proper antitumor action. Since mycobacteria are characterized by a rich lipid fraction on the cell surface,^{37,38} changes in the mycobacterial lipid content after growth in each culture medium may be involved in the different antitumor effects observed.

M. brumae and BCG share the structural skeleton common to all mycobacteria, composed of arabinogalactan, peptidoglycan and mycolic acids, and the presence of some noncovalent linked lipids such as PIM, TDM, TMM and TAG that were present in the cell wall under all culture conditions (Figures 4 and 5). However, the outermost layer is enriched in specific lipids depending on the culture medium in which they are grown. Here, after a short exposition to an apolar solvent that permits the extraction of the outermost lipid molecules,¹⁴ a reduced variety of lipids was strikingly observed in the outermost layer of *M. brumae*-A60 and BCG-G15 compared to the rest of the cultures. Among all *M. brumae* cultures, *M. brumae*-

A60 was unique and showed only GroMM, while BCG-G15 showed less PDIM, PGL and GroMM located outside of the cell than the rest of the BCG cultures (Figures 4 and 5). The presence/absence of each of these lipids might be a determinant of the triggered immune response.

The first observation was the positive correlation between GroMM presence in the outermost layer and a high glycerol concentration in the culture medium, as previously described.³⁹ GroMM constitutes glycerol and a monomycolate acid^{39,40} and, like other mycolic acid (MA)-derived molecules (such as TDM or TMM), has been related to the cell hydrophobicity,⁴¹ persistence and virulence of pathogenic mycobacteria species,^{42–44} resistance to therapeutic agents⁴⁵ and immune system interaction. *M. brumae* presented only α -GroMM, while GroMM exposed on BCG corresponded to only keto-mycolic acid, although Connaught BCG contains α - and κ -mycolates. The presence of only κ -mycolic acid can be explained since its conformation is more stable than that acquired by α -mycolic acid.⁴⁶ GroMM is an immunostimulatory molecule that can be recognized by the human innate immune receptor macrophage-inducible C-type lectin (Mincle), which leads to a proinflammatory response including synthesis of NO, modulation of Toll-like receptor 2-mediated cytokine responses and release of proinflammatory cytokines,^{47–49} independent of the α - or κ -mycolic acid content.⁵⁰ Although the R-isomer from BCG has been described as more reactive than the S-isomer,⁵¹ a mixture of both isomers was found in our mycobacterial extracts. Moreover, although initial reports found that GroMM does not bind to the mouse Mincle receptor, in contrast to human Mincle, recent research and preliminary results from our laboratory indicate that GroMM can bind to the mouse Mincle receptor at higher concentrations,⁵² explaining the observed immune response triggered by *M. brumae*-A60. Moreover, *M. brumae*-A60 was specifically devoid of AGs on the cell surface, although the ultrastructural analysis and total lipidic profile of *M. brumae* showed the presence of AGs. AG accumulation could occur as peripheral deposits associated with the cell envelope and in ILIs,⁵³ both in *M. tuberculosis* and nontuberculous mycobacteria.^{54,55} In *M. tuberculosis*, produced AGs are either transported towards the outer cell wall through the cytosol or accumulate in the cytosol as ILIs. Overexpression of an efflux pump and the membrane lipoprotein LprG/Rv1410 is responsible for the release of AG into culture medium,^{56,57} enabling the resistance of mycobacteria in the host immune environment. The function of surface-exposed AG on nontuberculous mycobacteria, such as *M. brumae*, with host interactions is still unknown. Experiments with *Mycobacterium abscessus* indicated that the presence of AG in the cell wall is not associated with excess AG storage in ILIs.⁵⁸ Nonetheless, it could also be hypothesized that AG absence on *M. brumae*-A60 could favor the interaction of host receptors with PAMPs. Further studies are needed to elucidate the unknown functions of AG.

In BCG-G15, the diminished amounts of PDIM and PGL compared to the amounts found in the rest of the BCG cultures could be a determinant of its efficacy. PDIM and PGL are present in only a selected group of mycobacteria, such as *M. tuberculosis*, *Mycobacterium marinum*, and some strains of BCG.^{59,60} PDIM is required for *M. tuberculosis* and *M.*

marinum virulence in mouse and zebrafish models, respectively,^{45,61–65} mycobacterial persistence in host tissues mediated by inhibiting phagosome maturation⁶⁶ and disease dissemination.⁶⁷ PDIM interacts with host membranes to remodel lipid organization,^{68–70} interferes with IFN- γ -independent host defense,⁷¹ and masks mycobacterial PAMPs, affecting innate immune signaling pathways.⁷² Infection with PDIM-mutant strains induced dendritic cells and macrophages to secrete more tumor necrosis factor (TNF)- α and interleukin (IL)-6 than infection with the wild-type strain.⁷³ Likewise, PGL has been associated with the *M. tuberculosis* hypervirulent phenotype, inhibiting host production of proinflammatory cytokines such as TNF- α , IL-6 and IL-1 β .^{74–76} Moreover, both compounds also play a role in cell wall permeability since mutants lacking PDIM and PGL are more sensitive to various hydrophobic and hydrophilic drugs.⁷⁷ In the case of BCG, the presence of PDIM and/or PGL varies among BCG substrains,⁷⁸ yet few works associate their presence with a specific role when using BCG as an immunomodulatory agent. In the context of tuberculosis protection, PDIM present on the BCG Pasteur substrain cell wall is needed for complete protection against *M. tuberculosis* challenge in mouse models,⁷⁶ although a PDIM/PGL-mutant strain did not alter the release of IFN- γ by CD4 and CD8 T cells compared to the wt strain. In the context of BC, the roles of these antigens are known. Our work demonstrates that the antitumor effect is enhanced when the amount of these compounds is diminished in the BCG cell wall. Although a direct relationship between PDIM/PGL presence in BCG substrains and BC growth inhibition *in vitro* has not been observed,⁷⁸ the presence of PDIM/PGL could modify the interactions of PAMPs with immune cells or even alter cell permeability, allowing the release of other antigens with immunomodulatory effects.

Moreover, the profile of the outermost lipidome can influence the antitumor effect not only via a direct interaction with immune receptors but also by altering the physicochemical properties of the mycobacteria that modify the host-mycobacteria interaction. Our results show that BCG-G15, in contrast to the rest of the BCG cultures, was not able to take the neutral red stain in its non-ionic hydrophobic form due to a non-adherence on mycobacteria surface and/or the lack of compounds with reducing power on the cells. The variation on the hydrophobicity and/or charge on the cell surface of mycobacteria cells,⁷⁹ could be an advantage when interacting with BC cells. In contrast to normal bladder cells, tumor cells contain a diminished amount of sulfated glycosaminoglycan (GAGs), which alter the physicochemical characters of the cells.⁸⁰ Thus, BCG-G15 could be properly attached to tumor cells. Additionally, it is plausible that the exposure of fibronectin-binding proteins involved in the interactions between *M. brumae* or BCG and tumor cells⁸¹ could be altered as a function of the mycobacterial surface lipidome.

In our experiments, mycobacteria were meticulously harvested at the same time from all mycobacterial cultures to assess the influence of the culture conditions on the mycobacterial antitumor effect. However, the lipidic profile is built in a time-dependent manner as a function of the environmental and nutritional statuses of the cells.⁸² In view of our results, it

could be of interest to recover cultured mycobacteria at different time points to unravel the role of each lipid profile and decipher the convenient antigenic profile for enhancing a desired immunostimulatory activity. Moreover, we have studied the BCG Connaught substrain, but the influence of the culture medium used for manufacturing other BCG substrains devoid of PDIM and PGL glycolipids in clinical use is unknown. Similar to BCG Connaught, other BCG substrains showed a diminished lipidic content on the outermost cell surface when culture in G15 medium.⁷⁹ Accordingly, another interesting point will also be to study different BCG substrains to investigate whether these lipids or other types of molecules are specifically responsible for the immune response. To understand how mycobacteria helps the immune system could be relevant for the selection of other bacterial species to treat patients following the current immunotherapy regimen, or in combination with new immunotherapy agents such as checkpoint inhibitors.⁸³

Our study had some limitations. First, only female mice were used. Because anatomic characteristics make mycobacterial treatment modeling in male mice impractical, differences in sex could influence the response to treatment, modifying the results obtained here.⁸⁴ The MB49 cell line used to induce tumor in mice generates aggressive bladder tumors compare to those treated with mycobacteria in BC patients. Moreover, the different immune systems between mice and humans also limited our conclusions. The fact that mice are devoid of group 1 CD1 molecules prevented us from determining whether surface-exposed mycolate-derived antigens have a role in triggering the adaptive immune response. After demonstrating here the surface exposure of some mycolic acid-derived antigens, further work with humanized mouse models with those receptors will shed light on these newly generated questions.⁸⁵

Overall, we have demonstrated that the mycobacterial lipidome depends on the culture conditions and that these profiles impact the triggered immune response, both local and systemic, when using mycobacteria for BC treatment, suggesting that the mycobacterial lipidome could be one of the factors influencing the success of the antitumor effect. Based on the data described here, we can conclude that the outcome of NMIBC depends not only on patient and/or tumor characteristics but also on mycobacterial characteristics that can be modulated as a function of the growth conditions. This evidence strengthens the understanding of the mechanism of action of mycobacteria in cancer treatment, providing new insights to improve this approach.

Conclusions

Growth conditions can impact the antitumor effect of BCG strains and could be a key parameter of treatment success. Tumor-bearing mouse survival, the splenocyte antitumor effect, and immune cell infiltration into tumors in mycobacteria-treated mice differed as a function of the culture conditions for each mycobacterial strain. Our data reveal that the mycobacterial surface is modified by culture conditions, suggesting an influence on the antitumor immune response triggered. These findings contribute to understanding the

antitumor mechanism of mycobacteria, allowing improved management of BC patients.

List of abbreviations

BC, Bladder Cancer
 BCG, *Mycobacterium bovis* bacillus Calmette-Guérin
 BSA, Bovine Serum Albumin
 CDCl₃, Deuterate chloroform
 CFU, Colony Forming Units
 CO₂, Carbon dioxide
 ConA, Concanavalin A
 DMEM, Dulbecco's modified Eagle's medium
 ELISA, Enzyme-linked Immunosorbent Assay
 FBS, Fetal Bovine Serum
 GAG, Glycosaminoglycans
 GroMM, Glycerol Monomycolate
¹H NMR, Proton Nuclear Magnetic Resonance
¹H, ¹H-COSY, Correlation Spectroscopy
¹H, ¹³C-HSQC, Heteronuclear Single Quantum Coherence
 Ig, Immunoglobulin
 IL, Interleukin
 ILC, Innate Lymphoid Cells
 IFN- γ , Interferon- γ
M. brumae, *Mycobacterium brumae*
 MTT, Thiazolyl blue tetrazolium bromide
 NF- κ B, Nuclear Factor - κ B
 NK, Natural Killer
 NMIBC, Non-Muscle Invasive Bladder Cancer
 NMR, Nuclear Magnetic Resonance
 PBS, Phosphate Buffered Saline
 PDIM, Phtiocerol dimycocerosates
 PGL, Phenol Glycolipid
 PE, Petroleum Ether
 OD, Optical Density
 RPMI 1640, Roswell Park Memorial Institute 1640
 SD, Standard Deviation
 SEM, Scanning Electron microscopy
 T_{EM}, Effector Memory CD4⁺ T cells
 TLC, Thin-layer chromatography
 TNF- α , Tumour Necrosis Factor- α

Acknowledgments

We are grateful to the technical staff from the Estabulari UAB for their outstanding animal management. We thank the IGTP Cytometry Core Facility and Marco Antonio Fernández for his contribution to this publication. Graphical abstract was created with Biorender.com.

Ethics approval

In vivo experiments were performed in accordance with national and European Union legislation regarding the protection of experimental animals, and were reviewed by the Animal Care Committee at the Autonomous University of Barcelona and the Catalonia government (project 9171) and approved by the Departament d'Agricultura, Ramaderia, Pesca, Alimentació i Medi Natural of the Catalan Regional Government. Mice were supervised following a strict monitoring protocol in order to ensure animal welfare, and euthanized, if required.

Consent for publication

Not applicable

Availability of data and materials

All data generated or analysed during this study are included in this published article [and its supplementary information files].












Disclosure statement

No potential conflict of interest was reported by the author(s).

Funding

This work was funded by the Spanish Ministry of Science, Innovation and Universities grant RTI2018-098777-B-I00 (EJ) and FEDER Funds (EJ), Generalitat of Catalunya grant 2017SGR-229 (EJ, ML), Generalitat de Catalunya PhD contracts FI (SG-G, VC-P).

ORCID

Sandra Guallar-Garrido  <http://orcid.org/0000-0002-9666-5757>
 Víctor Campo-Pérez  <http://orcid.org/0000-0003-3161-9984>
 Míriam Pérez-Trujillo  <http://orcid.org/0000-0002-6919-7417>
 Cecilia Cabrera  <http://orcid.org/0000-0002-9941-6828>
 Jordi Senserrich  <http://orcid.org/0000-0002-8021-1718>
 Alejandro Sánchez-Chardi  <http://orcid.org/0000-0002-8789-1883>
 Rosa Maria Rabanal  <http://orcid.org/0000-0002-9521-791X>
 Elisabet Gómez-Mora  <http://orcid.org/0000-0002-9779-5940>
 Estela Noguera-Ortega  <http://orcid.org/0000-0001-6507-0673>
 Marina Luquin  <http://orcid.org/0000-0002-6015-3282>
 Esther Julián  <http://orcid.org/0000-0002-6558-3978>

Authors' contributions

Conceptualization, S.G.-G. and E.J.; Formal Analysis, S.G.-G., V.C.P., M.P.T., C.C., J.S.; Investigation, S.G.-G., V.C.P., M.P.T., C.C., J.S., A.S.Ch., R.R., E.G.-M., E.N.-O., M.L. and E.J.; Data Curation, S.G.-G.; Writing –Original Draft Preparation, S.G.-G., C.C., M.L., and E.J.; Writing –Review & Editing Preparation, all authors; Visualization Preparation, all authors; Supervision, Project Administration and Funding Acquisition EJ.

References

- Babjuk M, Burger M, Zigeuner R, Shariat SF, van Rhijn BWG, Compérat E, Hernández V, Kaasinen E, Palou J, Roupřt M, *et al.* EAU guidelines on non-muscle-invasive urothelial carcinoma of the bladder: update 2013. *Eur Urol.* 2013;64:639–653. doi:10.1016/j.eururo.2013.06.003.
- Sfakianos JP, Salome B, Daza J, Farkas A, Bhardwaj N, Horowitz A. Bacillus Calmette-Guerin (BCG): its fight against pathogens and cancer. *Urol Oncol.* 2021;39:121–129. doi:10.1016/j.urolonc.2020.09.031.
- Brausi M, Oddens J, Sylvester R, Bono A, Van De Beek C, Van Andel G, Gontero P, Turkeri L, Marreaud S, Collette S, *et al.* Side effects of bacillus calmette-guérin (BCG) in the treatment of intermediate- and high-risk Ta, T1 papillary carcinoma of the bladder: results of the EORTC genito-urinary cancers group randomised phase 3 study comparing one-third dose with full dose. *Eur Urol.* 2014;65:69–76. doi:10.1016/j.eururo.2013.07.021.
- Noguera-Ortega E, Secanella-Fandos S, Eraña H, Gasión J, Rabanal RM, Luquin M, Torrents E, Julián E. Nonpathogenic *Mycobacterium brumae* inhibits bladder cancer growth in vitro, ex vivo, and in vivo. *Eur Urol Focus.* 2016;2:67–76. doi:10.1016/j.euf.2015.03.003.
- Noguera-Ortega E, Rabanal RM, Gómez-Mora E, Cabrera C, Luquin M, Julián E. Intravesical *Mycobacterium brumae* triggers both local and systemic immunotherapeutic responses against bladder cancer in mice. *Sci Rep.* 2018;8:15102. doi:10.1038/s41598-017-18329-3.

6. Bach-Griera M, Campo-Pérez V, Barbosa S, Traserra S, Guallar-Garrido S, Moya-Andérico L, Herrero-Abadía P, Luquin M, Rabanal RM, Torrents E, et al. *Mycolicobacterium brumae* is a safe and non-toxic immunomodulatory agent for cancer treatment. *Vaccines*. 2020;8:2–17. doi:10.3390/vaccines8020198.
7. Sylvester RJ, Van Der Meijden APM, Oosterlinck W, Witjes JA, Boufflioux C, Denis L, Newling DWW, Kurth K. Predicting recurrence and progression in individual patients with stage Ta T1 bladder cancer using EORTC risk tables: a combined analysis of 2596 patients from seven EORTC trials. *Eur Urol*. 2006;49:466–477. doi:10.1016/j.eururo.2005.12.031.
8. Dagogo-Jack I, Shaw AT. Tumour heterogeneity and resistance to cancer therapies. *Nat Rev Clin Oncol*. 2018;15:81–94. doi:10.1038/nrclinonc.2017.166.
9. Wei H, Kamat A, Chen M, Ke HL, Chang DW, Yin J, Grossman HB, Dinney CP, Wu X. Association of polymorphisms in oxidative stress genes with clinical outcomes for bladder cancer treated with bacillus Calmette-Guérin. *PLoS One*. 2012;7:e38533. doi:10.1371/journal.pone.0038533.
10. Lima L, Oliveira D, Ferreira JA, Tavares A, Cruz R, Medeiros R, Santos L. The role of functional polymorphisms in immune response genes as biomarkers of bacille Calmette-Guérin (BCG) immunotherapy outcome in bladder cancer: establishment of a predictive profile in a Southern Europe population. *BJU Int*. 2015;116:753–763. doi:10.1111/bju.12844.
11. Guallar-Garrido S, Campo-Pérez V, Sánchez-Chardi A, Luquin M, Julián E. Each mycobacterium requires a specific culture medium composition for triggering an optimized immunomodulatory and antitumoral effect. *Microorganisms*. 2020;8:734. doi:10.3390/microorganisms8050734.
12. Pettenati C, Ingersoll MA. Mechanisms of BCG immunotherapy and its outlook for bladder cancer. *Nat Rev Urol*. 2018;15:615–625. doi:10.1038/s41585-018-0055-4.
13. Julián E, Noguera-Ortega E. *Microb Infect Cancer Ther Recent Adv*. 1st ed. 2019. *Bacteria-Derived Alternatives to Live Mycobacterium bovis Bacillus Calmette-Guérin for Nonmuscle Invasive Bladder Cancer Treatment*; Chakrabarty AM, Fialho AM, eds; (Boca Raton: Jenny Stanford Publishing) :123–188. doi:10.1201/9781351041904.
14. Llorens-Fons M, Pérez-Trujillo M, Julián E, Brambilla C, Alcaide F, Byrd TF, Luquin M. Trehalose polyphleates, external cell wall lipids in *Mycobacterium abscessus*, are associated with the formation of clumps with cording morphology, which have been associated with virulence. *Front Microbiol*. 2017;8:1402. doi:10.3389/fmicb.2017.00008.
15. Guallar-Garrido S, Luquin M, Julián E. Analysis of the lipid composition of mycobacteria by thin layer chromatography. *J Vis Exp*. 2021;1–17 doi:10.3791/62368.
16. Llorens-Fons M, Julián E, Luquin M, Pérez-Trujillo M. Molecule confirmation and structure characterization of pentatriacontatrienyl mycolate in *Mycobacterium smegmatis*. *Chem Phys Lipids*. 2018;212:138–143. doi:10.1016/j.chemphyslip.2017.12.006.
17. Soto CY, Andreu N, Gibert I, Luquin M. Simple and rapid differentiation of *Mycobacterium tuberculosis* H37Ra from *M. tuberculosis* clinical isolates through two cytochemical tests using neutral red and Nile blue stains. *J Clin Microbiol*. 2002;40:3021–3024. doi:10.1128/JCM.40.8.3021-3024.2002.
18. Layre E, Collmann A, Bastian M, Mariotti S, Czaplicki J, Prandi J, Mori L, Stenger S, De Libero G, Puzo G et al. Mycolic acids constitute a scaffold for mycobacterial lipid antigens stimulating CD1-Restricted T Cells. *Chem Biol*. 2009;16:82–92 doi:10.1016/j.chembiol.2008.11.008.
19. Brambilla C, Sánchez-Chardi A, Pérez-Trujillo M, Julián E, Luquin M. Cyclopropanation of α -mycolic acids is not required for cording in *Mycobacterium brumae* and *Mycobacterium fallax*. *Microbiology*. 2012;158:1615–1621. doi:10.1099/mic.0.057919-0.
20. Tabouret P, Astarie-Dequeker C, Demangel C, Malaga W, Constant P, Ray A, Honoré N, Bello NF, Pérez E, Daffé M et al. *Mycobacterium leprae* phenolglycolipid-1 expressed by engineered *M. bovis* BCG modulates early interaction with human phagocytes. *PLoS Pathog*. 2010;6:e1001159. doi:10.1371/journal.ppat.1001159.
21. Cardona PJ, Soto CY, Martín C, Giquel B, Agustí G, Guirado E, Sirakova T, Kolattukudy P, Julián E, Luquin M. Neutral-red reaction is related to virulence and cell wall methyl-branched lipids in *Mycobacterium tuberculosis*. *Microbes Infect*. 2006;8:183–190. doi:10.1016/j.micinf.2005.06.011.
22. Dowell AC, Cobby E, Wen K, Devall AJ, During V, Anderson J, James ND, Cheng KK, Zeegers MP, Bryan RT et al. Interleukin-17-positive mast cells influence outcomes from BCG for patients with CIS: data from a comprehensive characterisation of the immune microenvironment of urothelial bladder cancer. *PLoS One*. 2017;12:e0184841. doi:10.1371/journal.pone.0184841.
23. Takeuchi A, Dejima T, Yamada H, Shibata K, Nakamura R, Eto M, Nakatani T, Naito S, Yoshikai Y. IL-17 production by $\gamma\delta$ T cells is important for the antitumor effect of *Mycobacterium bovis* bacillus Calmette-Guérin treatment against bladder cancer. *Eur J Immunol*. 2011;41:246–251. doi:10.1002/eji.201040773.
24. Spits H, Artis D, Colonna M, Diefenbach A, Di Santo JP, Eberl G, Koyasu S, Locksley RM, McKenzie ANJ, Mebius RE, et al. Innate lymphoid cells—a proposal for uniform nomenclature. *Nat Rev Immunol*. 2013;13:145–149. doi:10.1038/nri3365.
25. Takatori H, Kanno Y, Watford WT, Tato CM, Weiss G, Ivanov II, Ivanov II, Littman DR, O’Shea JJ. Lymphoid tissue inducer – like cells are an innate source of IL-17 and IL-22. *J Exp Med*. 2009;206:35–41. doi:10.1084/jem.20072713.
26. Ghaedi M, Ohashi PS. ILC transdifferentiation: roles in cancer progression. *Cell Res*. 2020;30:562–563. doi:10.1038/s41422-020-0326-5.
27. Ercolano G, Falquet M, Vanoni G, TrabANELLI S, Jandus C. ILC2s: new actors in tumor immunity. *Front Immunol* 10:2801. 2019. doi:10.3389/fimmu.2019.02801.
28. Crinier A, Vivier E, Bléry M. Helper-like innate lymphoid cells and cancer immunotherapy. *Semin Immunol*. 2019;41:101274. doi:10.1016/j.jsmim.2019.04.002.
29. Bruchard M, Ghiringhelli F. Deciphering the roles of innate lymphoid cells in cancer. *Front Immunol*. 2019;10:656. doi:10.3389/fimmu.2019.00656.
30. Chevalier MF, TrabANELLI S, Racle J, Salomé B, Cesson V, Gharbi D, Bohner P, Domingos-Pereira S, Dartiguenave F, Fritschi A-S, et al. ILC2-modulated T cell-to-MDSC balance is associated with bladder cancer recurrence. *J Clin Invest*. 2017;127:2916–2929. doi:10.1172/JCI89717.
31. Allan DSJ, Cerdeira AS, Ranjan A, Kirkham CL, Aguilar OA, Tanaka M, Childs RW, Dunbar CE, Strominger JL, Kopcow HD, et al. Transcriptome analysis reveals similarities between human blood CD3⁺ CD56⁺ bright cells and Transcriptome analysis reveals similarities between human blood CD3⁺ CD56^{bright} cells and mouse CD127⁺ innate lymphoid cells. *Sci Rep*. 2017;7:3501. doi:10.1038/s41598-017-03256-0
32. García-Cuesta EM, Estes G, Ashiru O, López-Cobo S, Álvarez-Maestro M, Linares A, Ho, MM, Martínez-Piñeiro L, Reyburn H, Valés-Gómez M, et al. Characterization of a human anti-tumoral NK cell population expanded after BCG treatment of leukocytes. *Oncoimmunology* 6. 2017:e1293212 doi:10.1080/2162402X.2017.1293212.
33. Annels NE, Simpson GR, Pandha H. Modifying the non-muscle invasive bladder cancer immune microenvironment for optimal therapeutic response. *Front Oncol*. 2020;10:10. doi:10.3389/fonc.2020.00010.
34. Guallar-Garrido S, Julián E. Bacillus Calmette-Guérin (BCG) therapy for bladder cancer: an update. *ImmunoTargets Ther*. 2020;9. doi:10.2147/ITT.S202006.
35. Kamat AM, Flaig TW, Grossman HB, Konety B, Lamm D, O’Donnell MA, Uchio, E, Efstathiou, JA, Taylor, JA 3rd. Expert consensus document: consensus statement on best practice management regarding the use of intravesical immunotherapy with BCG for bladder cancer. *Nat Rev Urol*. 2015;12:225–235 doi:10.1038/nrurol.2015.58.

36. Pichler R, Fritz J, Zavadil C, Schäfer G, Culig Z, Brunner A. Tumor-infiltrating immune cell subpopulations influence the oncologic outcome after intravesical bacillus calmette-guérin therapy in bladder cancer. *Oncotarget*. 2016;7:39916–39930 doi:10.18632/oncotarget.9537.
37. Chiaradia L, Lefebvre C, Parra J, Marcoux J, Bulet-Schiltz O, Etienne G, Tropis M, Daffé M. Dissecting the mycobacterial cell envelope and defining the composition of the native mycomembrane. *Sci Rep*. 2017;7. doi:10.1038/s41598-017-12718-4.
38. Ortalo-Magné A, Dupont M-A, Lemassu A, Andersen AB, Gounon P, Daffé M. Molecular composition of the outermost capsular material of the tubercle bacillus. *Microbiology*. 1995;141(7):1609–1620. doi:10.1099/13500872-141-7-1609.
39. Hattori Y, Morita D, Fujiwara N, Mori D, Nakamura T, Harashima H, Yamasaki S, Sugita M Glycerol monomycolate is a novel ligand for the human, but not mouse macrophage inducible C-type lectin Mincle. *J Biol Chem*. 2014;289:15405–15412 doi:10.1074/jbc.M114.566489.
40. Andersen CS, Agger EM, Rosenkrands I, Gomes JM, Bhowruth V, Gibson KJC, Petersen RV, Minnikin DE, Besra GS, Andersen P, et al. A simple mycobacterial monomycolated glycerol lipid has potent immunostimulatory activity. *J Immunol*. 2009;182:424–432. doi:10.4049/jimmunol.182.1.424.
41. Ojha AK, Trivelli X, Guerardel Y, Kremer L, Hatfull GF. Enzymatic hydrolysis of trehalose dimycolate releases free mycolic acids during mycobacterial growth in biofilms. *J Biol Chem*. 2010;285:17380–17389 doi:10.1074/jbc.M110.112813.
42. Clifton EB, Lee RE, Mdluli K, Sampson AE, Schroeder BG, Slayden RA 1998 .Mycolic acids: structure, biosynthesis and physiological functions *Prog Lipid Res* 37 143–79 doi:10.1016/s0163-7827(98)00008-3 .
43. Medjahed H, Gaillard J-L, Reyat J-M. *Mycobacterium abscessus*: a new player in the mycobacterial field. *Trends Microbiol*. 2010;18:117–123. doi:10.1016/j.tim.2009.12.007.
44. Vander Beken S, Al Dulayymi JR, Naessens T, Koza G, Maza-Iglesias M, Rowles R, Theunissen C, De Medts J, Lanckacker E, Baird MS, et al. Molecular structure of the *Mycobacterium tuberculosis* virulence factor, mycolic acid, determines the elicited inflammatory pattern. *Eur J Immunol*. 2011;41:450–460. doi:10.1002/eji.201040719.
45. Jackson M. The mycobacterial cell envelope-lipids. *Cold Spring Harb Perspect Med*. 2014;4:a021105. doi:10.1101/cshperspect.a021105.
46. Sambandan D, Dao DN, Weinrick BC, Vilchèze C, Gurcha SS, Ojha A, Kremer L, Besra GS, Hatfull GF, Jacobs WR. Keto-mycolic acid-dependent pellicle formation confers tolerance to drug sensitive drug-sensitive *Mycobacterium tuberculosis*. *MBio*. 2013;4:1–10. doi:10.1128/mBio.00222-13.
47. Richardson MB, Williams SJ, Agostino M, Zwirner NW. MCL and Mincle: c-type lectin receptors that sense damaged self and pathogen-associated molecular patterns. *Front Immunol*. 2014;5. doi:10.3389/fimmu.2014.00288.
48. Bin LW, Kang JS, Choi WY, Zhang Q, Kim CH, Choi UY, Kim-Ha J, Kim YJ . Mincle-mediated translational regulation is required for strong nitric oxide production and inflammation resolution. . *Nat Commun*. 2016;7:1–14 doi:10.1038/ncomms11322.
49. Patin EC, Willcocks S, Orr S, Ward TH, Lang R, Schaible UE. Mincle-mediated anti-inflammatory IL-10 response counter-regulates IL-12 in vitro. *Innate Immun*. 2016;22:181–185. . doi:10.1177/1753425916636671.
50. Andersen CAS, Rosenkrands I, Olsen AW, Nordly P, Christensen D, Lang R, Kirschning C, Gomes JM, Bhowruth V, Minnikin DE, et al. Novel generation mycobacterial adjuvant based on liposome-encapsulated monomycoloyl glycerol from mycobacterium bovis bacillus calmette-guérin. *J Immunol*. 2009;183:2294–2302. doi:10.4049/jimmunol.0804091.
51. Ali OT, Sahb MM, Al Dulayymi JR, Baird MS. Glycerol mycolates from synthetic mycolic acids. *Carbohydr Res*. 2017;448:67–73. doi:10.1016/j.carres.2017.04.023.
52. Iizasa E, Chuma Y, Uematsu T, Kubota M, Kawaguchi H, Umemura M, Toyonaga, K, Kiyohara, H, Yano, I, Colonna, M, et al. TREM2 is a receptor for non-glycosylated mycolic acids of mycobacteria that limits anti-mycobacterial macrophage activation. *Nat Commun* 12 2299 doi:10.1038/s41467-021-22620-3 . 2021.
53. Christensen H, Garton NJ, Horobin RW, Minnikin DE, Barer MR. Lipid domains of mycobacteria studied with fluorescent molecular probes. *Mol Microbiol*. 1999;31:1561–1572 doi:10.1046/j.1365-2958.1999.01304.x.
54. Bansal-Mutalik R, Nikaido H. Mycobacterial outer membrane is a lipid bilayer and the inner membrane is unusually rich in diacyl phosphatidylinositol dimannosides. *Proc Natl Acad Sci USA*. 2014;111:4958–4963. doi:10.1073/pnas.1403078111.
55. Ortalo-Magné A, Lemassu A, Lanéelle MA, Bardou F, Silve G, Gounon P, Marchal G, Daffé M. Identification of the surface-exposed lipids on the cell envelopes of *Mycobacterium tuberculosis* and other mycobacterial species. *J Bacteriol*. 1996;178:456–461. doi:10.1128/jb.178.2.456-461.1996.
56. Martinot AJ, Farrow M, Bai L, Layre E, Cheng T-Y, Tsai JH, Iqbal J, Annand JW, Sullivan ZA, Hussain MM *et al* . PLoS Pathog. 12. ; 2016 Mycobacterial Metabolic Syndrome: lprG and Rv1410 Regulate Triacylglyceride Levels, Growth Rate and Virulence in *Mycobacterium tuberculosis* . e1005351 doi:10.1371/journal.ppat.1005351.
57. Maurya RK, Bharti S, Krishnan MY. Triacylglycerols: fuelling the Hibernating *Mycobacterium tuberculosis*. *Front Cell Infect Microbiol*. 2019;8:450. doi:10.3389/fcimb.2018.00450.
58. Viljoen A, Blaise M, de Chastellier C, Kremer L. MAB_3551c encodes the primary triacylglycerol synthase involved in lipid accumulation in *Mycobacterium abscessus*. *Mol Microbiol*. 2016;102:611–627 doi:10.1111/mmi.13482.
59. Batt SM, Minnikin DE, Besra GS. The thick waxy coat of mycobacteria, a protective layer against antibiotics and the host's immune system. *Biochem J*. 2020;447:1983–2006 doi:10.1042/BCJ20200194.
60. Minnikin DE, Brennan PJ. Health Consequences of Microbial Interactions with Hydrocarbons, Oils, and Lipids 1 Goldfine H (Springer, Cham) . 2020 Lipids of Clinically Significant Mycobacteria ; 33–108 doi:https://doi.org/10.1007/978-3-030-15147-8 .
61. Osmá MM, Paga AJ, Shanaha JK, Ramakrishnan L. *Mycobacterium marinum* phthiocerol dimycocerosates enhance macrophage phagosomal permeabilization and membrane damage. *PLoS One* 15 . 2020;:e0233252 doi:10.1371/journal.pone.0233252.
62. Camacho LR, Ensergueix D, Perez E, Gicquel B, Guilhot C. Identification of a virulence gene cluster of *Mycobacterium tuberculosis* by signature-tagged transposon mutagenesis. *Mol Microbiol*. 1999;34:257–267. . doi:10.1046/j.1365-2958.1999.01593.x.
63. Cox JS, Chess B, McNeil M, Jacobs WR. Complex lipid determines tissue-specific replication of *Mycobacterium tuberculosis* in mice. *Nature*. 1999;402:79–83 doi:10.1038/47042.
64. Passemar C, Arbués A, Malaga W, Mercier I, Moreau F, Lepourry L, Neyrolles O, Guilhot C, Astarie-Dequeker C. Multiple deletions in the polyketide synthase gene repertoire of *Mycobacterium tuberculosis* reveal functional overlap of cell envelope lipids in host-pathogen interactions. *Cell Microbiol*. 2014;16:195–213. doi:10.1111/cmi.12214.
65. Yu J, Tran V, Li M, Huang X, Niu C, Wang D, Zhu J, Wang J, Gao Q, Liu J, et al. Both phthiocerol dimycocerosates and phenolic glycolipids are required for virulence of *Mycobacterium marinum*. *Infect Immun*. 2012;80:1381–1389. doi:10.1128/IAI.06370-11.
66. Robinson N, Kolter T, Wolke M, Rybniker J, Hartmann P, Plum G. Mycobacterial phenolic glycolipid inhibits phagosome maturation and subverts the pro-inflammatory cytokine response. *Traffic*. 2008;9:1936–1947. 10.1111/doi:10.1111/j.1600-0854.2008.00804.x.

67. Quigley J, Hughitt VK, Velikovskiy CA, Mariuzza RA, El-Sayed NM, Briken V. The cell wall lipid PDIM contributes to phagosomal escape and host cell exit of *Mycobacterium tuberculosis*. *MBio*. 2017;8:e00148–17. doi:10.1128/mBio.00148-17.
68. Augenreich J, Haanappel E, Ferré G, Czaplicki G, Jolibois F, Destainville N, Guilhot C, Milon A, Astarie-Dequeker C, Chavent M, et al. The conical shape of DIM lipids promotes *Mycobacterium tuberculosis* infection of macrophages. *Proc Natl Acad Sci USA*. 2019;116:25649–25658. doi:10.1073/pnas.1910368116.
69. Augenreich J, Haanappel E, Sayes F, Simeone R, Guillet V, Mazeres S, Chalut C, Mourey L, Brosch R, Guilhot C, et al. Phthiocerol dimycocerosates from *Mycobacterium tuberculosis* increase the membrane activity of bacterial effectors and host receptors. *Front Cell Infect Microbiol*. 2020;10:420. doi:10.3389/fcimb.2020.00420.
70. Astarie-Dequeker C, Le Guyader L, Malaga W, Seaphanh F-K, Chalut C, López A, Guilhot C. PLoS Pathog. 52009 Phthiocerol dimycocerosates of *M. tuberculosis* participate in macrophage invasion by inducing changes in the organization of plasma membrane lipids. e1000289 doi:10.1371/journal.ppat.1000289.
71. Murry JP, Pandey AK, Sasseti CM, Rubin EJ. phthiocerol dimycocerosate transport is required for resisting interferon- γ -independent immunity. *J Infect Dis*. 2009;200:774–782. doi:10.1086/605128.
72. Cambier CJ, Takaki KK, Larson RP, Hernandez RE, Tobin DM, Urdahl KB, Cosma CL, Ramakrishnan L. Mycobacteria manipulate macrophage recruitment through coordinated use of membrane lipids. *Nature*. 2014;505:218–222. doi:10.1038/nature12799.
73. Rousseau C, Winter N, Privert E, Bordat Y, Neyrolles O, Avé P, Huerre M, Gicquel B, Jackson M. Production of phthiocerol dimycocerosates protects *Mycobacterium tuberculosis* from the cidal activity of reactive nitrogen intermediates produced by macrophages and modulates the early immune response to infection. *Cell Microbiol*. 2004;6:277–287. doi:10.1046/j.1462-5822.2004.00368.x.
74. Arbués A, Malaga W, Constant P, Guilhot C, Prandi J, Astarie-Dequeker C. Trisaccharides of phenolic glycolipids confer advantages to pathogenic mycobacteria through manipulation of host-cell pattern-recognition receptors. *ACS Chem Biol*. 2016;11:2865–2875. doi:10.1021/acscchembio.6b00568.
75. Elsaidi HRH, Lowary TL. Effect of phenolic glycolipids from *Mycobacterium kansasii* on proinflammatory cytokine release. A structure–activity relationship study. *Chem Sci*. 2015;6:3161–3172 doi:10.1039/c4sc04004j.
76. Tran V, Ahn SK, Ng M, Li M, Liu J. Loss of lipid virulence factors reduces the efficacy of the BCG vaccine. *Sci Rep*. 2016;6:29076 doi:10.1038/srep29076.
77. Camacho LR, Constant P, Raynaud C, Lanéelle MA, Triccas JA, Gicquel B, Daffé M, Guilhot C Analysis of the phthiocerol dimycocerosate locus of *Mycobacterium tuberculosis*. Evidence that this lipid is involved in the cell wall permeability barrier. *J Biol Chem*. 2001;276:19845–19854 doi:10.1074/jbc.M100662200.
78. Secanella-Fandos S, Luquin M, Julián E. Connaught and Russian strains showed the highest direct antitumor effects of different *Bacillus Calmette-Guérin* substrains. *J Urol*. 2013;189:711–718. doi:10.1016/j.juro.2012.09.049.
79. Guallar-Garrido S, Almiñana-Rapún F, Campo-Pérez V, Torrents E, Luquin M, Julián E. BCG Substrains change their outermost surface as a function of growth media. *Vaccines*. 2022;10:40 doi:10.3390/vaccines10010040.
80. Han J, Gu X, Li Y, Wu Q. Mechanisms of BCG in the treatment of bladder cancer-current understanding and the prospect. *Biomed Pharmacother* 129. 2020;110393 doi:10.1016/j.biopha.2020.110393.
81. Noguera-Ortega E, Blanco-Cabra N, Rabanal RM, Sánchez-Chardi A, Roldán M, Guallar-Garrido S, Torrents, E, Luquin, M, Julián, E. Mycobacteria emulsified in olive oil-in-water trigger a robust immune response in bladder cancer treatment. *Sci Rep*. 2016;6:27232. doi:10.1038/srep27232.
82. Garcia-Vilanova A, Chan J, Torrelles JB. Underestimated manipulative roles of *Mycobacterium tuberculosis* cell envelope glycolipids during infection. *Front Immunol* 10. 2019;2909 doi:10.3389/fimmu.2019.02909.
83. Kates M, Matoso A, Choi W, Baras AS, Daniels MJ, Lombardo K, Brant A, Mikkilineni N, McConkey DJ, Kamat AM *et al*. Adaptive immune resistance to intravesical BCG in non-muscle invasive bladder cancer: implications for prospective BCG-unresponsive trials. *Clin Cancer Res*. 2020;26:882–891 doi:10.1158/1078-0432.CCR-19-1920.
84. Rousseau M, O'Brien CJO, Antequera E, Zdimerova H, Cansever D, Canton T, Zychlinsky Scharff A, Ingersoll MA. Identification of sex differences in tumor-specific T cell infiltration in bladder tumor-bearing mice treated with BCG immunotherapy. *Bladder Cancer*. 2020;6(4):507–524. ; ; doi:10.3233/BLC-200384.
85. Eckhardt E, Bastian M. Animal models for human group 1 CD1 protein function. *Mol Immunol*. 2021;130:159–163. doi:10.1016/j.molimm.2020.12.018.